JACS
JOURNAL OF THE AMERICAN CHEMICAL SOCIETY
Communication
pubs.acs.org/JACS

Facile Synthesis of Palladium Right Bipyramids and Their Use as Seeds for Overgrowth and as Catalysts for Formic Acid Oxidation

Xiaohu Xia,[†] Sang-Il Choi,[†] Jeffrey A. Herron,[‡] Ning Lu,[∥] Jessica Scaranto,[‡] Hsin-Chieh Peng,[⊥] Jinguo Wang,[∥] Manos Mavrikakis,[‡] Moon J. Kim,[∥] and Younan Xia*[,†,⊥]

[†]The Wallace H. Coulter Department of Biomedical Engineering, Georgia Institute of Technology and Emory University, Atlanta, Georgia 30332, United States

[‡]Department of Chemical and Biological Engineering, University of Wisconsin-Madison, Madison, Wisconsin 53706, United States

[∥]Department of Materials Science and Engineering, University of Texas at Dallas, Richardson, Texas 75080, United States

[⊥]School of Chemistry and Biochemistry, Georgia Institute of Technology, Atlanta, Georgia 30332, United States

Supporting Information

ABSTRACT: Controlling the shape and thus facets of metal nanocrystals is an effective way to enhance their performance in catalytic reactions. While Pd nanocrystals with a myriad of shapes have been successfully prepared with good uniformity and in high yield, Pd right bipyramids (RBPs) that have a singly twinned structure have been elusive. We report a facile route based on polyol reduction for the synthesis of Pd RBPs with purity >90% and sizes controlled in the range 5−15 nm. The success of our synthesis relies on the use of iodide ions to manipulate the strength of an oxidative etchant and selectively cap the Pd{100} facets. The as-prepared RBPs could serve as seeds to generate a set of Pd nanocrystals with novel shapes and structures. The RBPs also exhibited enhanced catalytic activity toward formic acid oxidation, with a current density 2.5 and 7.1 times higher than those of the single-crystal Pd nanocubes (which were also mainly covered by {100} facets) and commercial Pd black, respectively.

Palladium nanocrystals have received great interest in recent years due to their remarkable performance in important catalytic reactions such as CO oxidation and alkene/alkyne hydrogenation, as well as C−C coupling reactions.[1] In general, the reactivity and selectivity of Pd nanocrystals for a certain catalytic reaction can be tailored by controlling their shape and thus the type of facets exposed on the surface.[1b,2] To this end, a wide variety of methods have been developed for the synthesis of Pd nanocrystals with different shapes, including cube, octahedron, bar, rod, wire, decahedron, icosahedron, and plate.[3] However, to our knowledge, Pd right bipyramids (RBPs) with a singly twinned structure in the middle have never been prepared with a percentage yield >30%. Although we and other groups have occasionally observed Pd RBPs as side products in some syntheses,[3c,d] it was extremely difficult to enrich them and thus investigate their properties. As demonstrated for both Ag and Au systems,[4] RBP is an interesting structure that can be conceived by symmetrically jointing two trirectangular tetrahedrons base-to-base. Accordingly, a RBP is covered by six right-isosceles triangular {100} facets and bisected by a very thin twin plane along the ⟨111⟩ direction. These unique surface and structural features make Pd RBPs particularly attractive for use as catalysts and as a new class of seeds for overgrowth.

Here we demonstrate that Pd RBPs can be prepared in >90% purity, with good uniformity, by using a polyol process, in which Na_2PdCl_4 was reduced by ethylene glycol (EG) at 160 °C in the presence of poly(vinyl pyrrolidone) (PVP) and NaI. PVP served as a stabilizer, while NaI acted as both an oxidative etchant for the selective removal of multiple-twinned Pd nanoparticles and a selective capping agent for the Pd{100} facets. The use of NaI at a proper concentration was the key to the production of high-quality Pd RBPs; increasing or reducing the concentration of NaI gave Pd nanocubes or multiple-twinned nanorods, respectively, as byproducts. Notably, the sizes of these Pd RBPs could be tuned from 5 to 15 nm simply by adjusting the reaction time. Potential applications of the Pd RBPs are demonstrated by employing them as seeds to generate Pd nanocrystals with exotic shapes that have not been observed before and as catalysts to catalyze formic acid oxidation with greatly enhanced activity relative to both Pd nanocubes and commercial Pd black.

In a standard synthesis, a solution of Na_2PdCl_4 in EG was rapidly injected (with a pipet) into a mixture containing PVP and NaI that had been preheated to 160 °C in air under magnetic stirring. After the addition of Na_2PdCl_4 for 2 h, the reaction was quenched with an ice/water bath (see Supporting Information for details). Figure 1A shows a typical transmission electron microscopy (TEM) image of the Pd RBPs prepared using the standard procedure. This image clearly shows that the Pd RBPs are uniform in both size and shape. An additional TEM image in Figure S1 demonstrates that the Pd RBPs could be obtained with >90% purity and in a relatively large quantity. Close examination indicates that the Pd RBPs have three major projected profiles: irregular tetragon, rhombus, and triangle. Figure 1B shows TEM images and 3D models of individual Pd RBPs in three common orientations corresponding to those labeled in Figure 1A. As indicated by the high-resolution (HR) TEM image in Figure 1C, the Pd RBP is bounded by {100} facets, similar to a single-crystal nanocube.[3a] The mirror symmetry of the bipyramid and its (100) side faces suggest that a (111) twin plane bisects its two trirectangular tetrahedra, which is confirmed by the HRTEM

Received: August 2, 2013
Published: October 9, 2013

   dx.doi.org/10.1021/ja408018j | J. Am. Chem. Soc. 2013, 135, 15706−15709

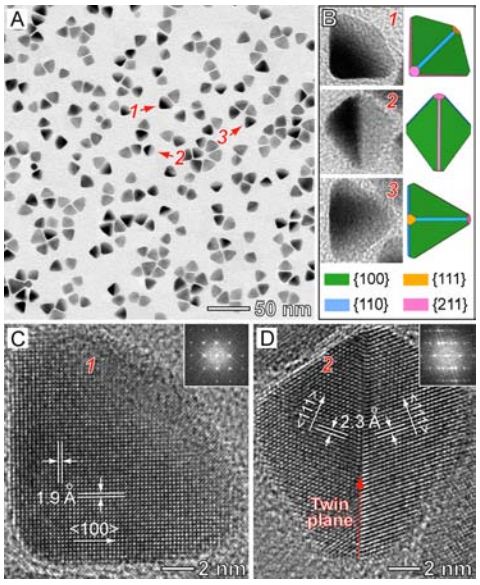

Figure 1. (A) TEM image of Pd RBPs prepared using the standard procedure. (B) TEM images and 3D models of individual Pd RBPs in three common orientations that correspond to the different projected shapes of RBPs marked with the same numbers as in panel A. In each model, green, yellow, blue, and pink denote {100}, {111}, {110}, and {211} facets, respectively. (C,D) HRTEM images taken from two individual Pd RBPs, whose orientations are the same as those marked with the same numbers in panels A and B. Insets: corresponding Fourier transform patterns.

image in Figure 1D. It is clear that each Pd RBP has six equivalent right-isosceles triangular (100) side faces (green in the 3D models) with an equilateral triangle as the base, in good agreement with what was observed in Ag RBPs.[4a,b] Interestingly, owing to the presence of a twin plane in the middle, both edges and corners of a Pd RBP can be categorized into two types: twin plane-free (type-*a*, blue and yellow in the 3D models) and twin plane-contained (type-*b*, pink in the 3D models). It is worth noting that the surfaces of type-*b* edges and corners can be assigned as high-index {211} facets, based on the ideal geometrical model of a RBP (Figure S2), and the average size of the Pd RBPs (defined as the length of a type-*a* edge) is 15 nm.

To clarify the formation mechanism of the Pd RBPs, aliquots of the reaction solution were taken from a standard synthesis at different reaction stages and examined using TEM. In the initial stage of the reaction (t = 1 min, Figure S3A), Pd nanoparticles with sizes of a few nanometers were formed. Analysis by HRTEM (see the inset of Figure S3A for a typical example) revealed that these nanoparticles exhibited an overall circular profile and contained a single twin defect, despite the fact that the twin plane is visible only at a specific orientation, making it difficult to determine their yield. At t = 5 min (Figure S3B), those small particles had grown into ca. 5 nm Pd RBPs, truncated at the corners. When the reaction time was prolonged to 20 min, 1 h, and 2 h, the average size of the Pd RBPs increased to 9, 13, and 15 nm, respectively (Figures 1A and S3C,D). Further extension of reaction time did not result in any obvious changes in either the size or shape. These results indicate that the Pd RBPs were essentially grown from small seeds containing single twin planes that were formed at the very early stage of a synthesis via homogeneous nucleation. In a sense, the size of the Pd RBPs could be controlled from 5 to 15 nm by quenching the reaction at different stages.

In the present synthesis, we found that the concentration of NaI played a crucial role in determining both the yield of RBPs and the types of byproducts. For example, the final products contained 5% RBPs and 95% single-crystal cubes (Figure 2A),

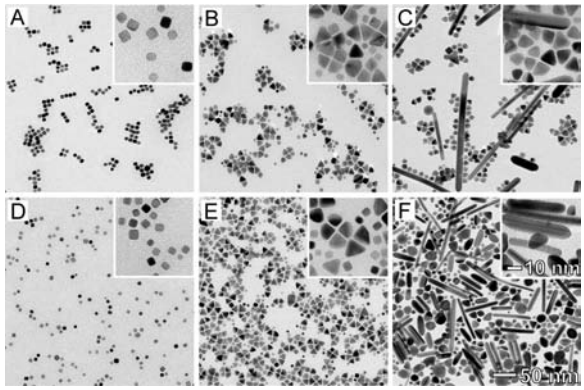

Figure 2. TEM images of Pd nanocrystals prepared using the standard procedure for the synthesis of Pd RBPs, except for the variation in the amount of NaI [(A) 600, (B) 300, and (C) 50 mg] and the bubbling of different gases through the reaction solution [(D) oxygen, (E) air, and (F) argon]. Insets: TEM images of the same samples at higher magnification. The scale bars in panel F apply to all images.

55% RBPs and 45% single-crystal cubes (Figure 2B), and 85% RBPs and 15% multiple-twinned rods (Figure 2C) when the amount of NaI was changed from 150 mg to 600, 300, and 50 mg, respectively. It can be concluded that the overall proportion of twin defects in the final products increased as the concentration of NaI decreased. These results can be attributed to the fact that halide ions can combine with O_2 from air to selectively etch away Pd nanoparticles with twin defects in the early stage of a polyol synthesis due to the relatively higher reactivity of twin defects.[5] It was also demonstrated that the strength of such oxidative etching had a direct correlation with the concentrations of both halide ions and O_2 in a polyol synthesis.[5b] As such, multiply twinned rods, which were most vulnerable to oxidative etching, could survive only at a relatively low concentration of I^- (Figure 2C); singly twinned RBPs could be obtained as the dominant species only at a moderate concentration of I^- (Figures 1A and 2B). All the twinned particles were dissolved when the concentration of I^- was sufficiently high, leaving behind single-crystal cubes (Figure 2A). In other words, the synthesis of Pd RBPs relies on the use of NaI to manipulate the strength of oxidative etching. It should be pointed out that results similar to those in Figure 2A–C were also obtained when NaI was replaced with the same amount of KI (data not shown), indicating that the I^- ions were mainly responsible for the formation of single-twinned RBPs.

To further validate the proposed mechanism of oxidative etching, another set of experiments was conducted, varying the concentration of O_2 by bubbling different gases through the standard reaction system. We found that Pd nanocrystals with shapes and twin structures similar to those shown in Figure 2A–C could still be obtained at reduced concentrations of O_2. As expected, single-crystal cubes (Figure 2D), a mixture of RBPs and single-crystal cubes (Figure 2E), and a mixture of RBPs and multiple-twinned rods (Figure 2F) were obtained when oxygen, air, and argon were bubbled through the reaction system, respectively. These results again support the proposed mechanism of oxidative etching. Just as Br^- ions can serve as a capping agent for the Pd{100} facets and thus facilitate the

dx.doi.org/10.1021/ja408018j | J. Am. Chem. Soc. 2013, 135, 15706–15709

formation of {100}-covered Pd nanocubes,[3a,6] we suspected that, in addition to the role of oxidative etching, I^- ions also acted as a capping agent specific to Pd(100) to promote the exposure of {100} facets on RBPs. We used X-ray photoelectron spectroscopy (XPS) to analyze the surface of the 15-nm Pd RBPs shown in Figure 1A, which were washed with deionized water four times to remove the physically adsorbed species. The XPS spectrum in Figure S4 shows an I 3d peak with relatively high intensity, detected from the Pd RBPs, implying the chemisorption of I^- ions onto the Pd(100) surface during the formation of RBPs. The final products became single-crystal Pd cuboctahedrons covered by a mix of {100} and {111} facets and nanocubes mainly covered by {100} facets when NaI was replaced by the same amount of NaCl and NaBr, respectively, while all other parameters were kept the same as the standard synthesis (Figure S5). These results imply that Cl^- ions had no capping effect for the Pd(100) surface, both I^- and Br^- ions could serve as Pd(100)-specific capping agents, and the oxidative etching power of Br^- ions was stronger than that of I^- ions, which facilitated the dissolution of singly twinned seeds and thus blocked the formation of Pd RBPs.

Seeded growth, in which newly formed atoms are added onto the surfaces of preformed seeds,[7] has emerged as a simple and powerful route to the synthesis of metal nanocrystals with controlled shapes. One of the most important principles in seeded growth is that the shape taken by the final product has a direct correlation with the twin structure of the seed.[8] Although the concept of seeded growth has been successfully applied to many types of seeds, including single-crystal polyhedrons, multiple-twinned decahedrons and icosahedrons, and plates containing stacking faults,[9] the growth of single-twinned seeds has not been reported. To this end, we employed the single-twinned Pd RBPs (Figure 1A) as seeds to investigate their growth habits. The seeded overgrowth was conducted by adding an aqueous Na_2PdCl_4 solution with a syringe pump into a mixture of ascorbic acid and Pd RBP seeds at room temperature (~22 °C) under magnetic stirring (see Supporting Information for details). We found that the growth was mainly confined to the ⟨211⟩ directions along the type-*b* corners of the RBPs, forcing the seeds to evolve into concave RBPs (Figure 3C). The preferential deposition of newly formed Pd atoms onto the type-*b* corners can be explained by the fact that these sites contain twin defects and thus should have a higher reactivity due to their higher surface free energies relative to the stable {111}-covered type-*a* corners and I^- ions-blocked side faces (Figure 3A,B). Our recent study demonstrated that surface diffusion plays a pivotal role in determining the growth pathway of a seed and thus the shape taken by the final product, which can be controlled by adjusting the reaction temperature.[10] The deposited atoms resulting from reduction of a precursor on a growing seed would migrate to other sites when the rate of surface diffusion ($V_{diffusion}$) is higher than that of atom deposition ($V_{deposition}$). We speculate that, at a sufficiently high reaction temperature, the atoms deposited at the type-*b* corners would migrate to edges and side faces of a Pd RBP seed during the growth process. As a result, the final products are supposed to take a shape of truncated bipyramid (Figure 3A,B). As expected, truncated bipyramids with an overall plate-like shape were indeed obtained when the reaction temperature was increased from 22 to 90 °C (Figure 3D). It is worth pointing out that the single-twinned defects were well retained after the overgrowth in both cases, as indicated by arrows in Figure 3C,D.

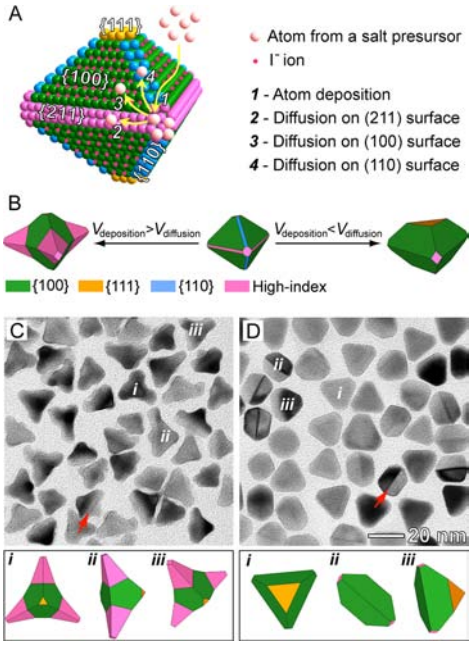

Figure 3. Schematic illustrations of (A) the pathway for adding Pd atoms onto the surface of a growing Pd RBP seed and (B) morphological evolutions of the Pd RBP seed under two different conditions. The size of I^- ions was reduced relative to Pd atoms to clearly show the surface structure. TEM images of Pd nanocrystals grown from the bipyramidal seeds at (C) 22 and (D) 90 °C; red arrows indicate the twin plane in final products. Below are shown 3D models of individual particles in three common orientations that correspond to the Pd nanocrystals marked with the same numbers in panels C and D, respectively. The scale bar in panel D also applies to panel C.

Finally, the 15-nm Pd RBPs were evaluated as catalyst for the electro-oxidation of formic acid. We benchmarked the catalytic activity of these Pd RBPs against 15-nm Pd nanocubes enclosed by {100} facets (Figure S6A) and commercial Pd black (Figure S6B). Prior to electrochemical measurements, the samples loaded on electrodes were treated with plasma etching for 30 min to remove the surface ligands (such as I^- ions, Figure S4) on the Pd catalysts. Note that both the shape and size of Pd RBPs were essentially retained during these treatments (Figure S7). In the first step, the electrochemically active surface area (ECSA) of these three types of Pd nanocrystals was determined from the charges associated with the stripping of a Cu monolayer underpotentially deposited (UPD) on their surfaces.[11] As shown in Figure S8, the two characteristic Cu_{UPD} current peaks for Pd{100} facets, at 0.42 and 0.56 V, were clearly resolved for the Pd nanocubes.[12] Although the Pd RBPs were also mainly covered by {100} facets, the first characteristic peak was broadened and the second was shifted to 0.57 V, likely due to the presence of twin defects and other facets on the Pd RBPs.[9d,13] Figure 4 shows cyclic voltammograms (CVs) normalized to the ECSAs of these three types of catalysts for electro-oxidation of formic acid. The Pd RBPs exhibited the highest specific electrocatalytic activity as compared to the Pd nanocubes and commercial Pd black, with 2.5 and 7.1 times increases for the peak current, respectively (see Table S2 for detailed data). Notably, the Pd RBPs also showed good catalytic stability, outperforming commercial Pd black (Figure S9). To understand the experimentally observed enhancement in catalytic activity of Pd RBPs relative to Pd cubes, we performed self-consistent periodic density functional theory (GGA-PW91) calculations (see

dx.doi.org/10.1021/ja408018j | J. Am. Chem. Soc. 2013, 135, 15706−15709

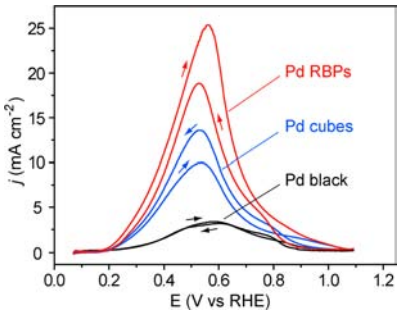

Figure 4. CVs of the 15-nm Pd RBPs (red in Figure 1A), 15-nm Pd cubes (blue in Figure S6A), and commercial Pd black (black in Figure S6B), recorded at room temperature in a N_2-saturated solution containing 0.5 M $HClO_4$ and 0.5 M HCOOH at a scan rate of 50 mV/s. The current density was normalized against the corresponding electrochemically active surface area. RHE = reversible hydrogen electrode.

Supporting Information for details). Since the Pd cubes were covered by {100} facets and the surface of Pd RBPs contained both {100} and {211} facets, we compared the reactivity between model Pd(100) and Pd(211) extended surfaces. Note that, unlike decahedrons and icosahedrons,[8a] the boundary region of a twin defect in a RBP is only a single strip of stacking fault, and essentially no disordered region other than (211) surface is exposed (Figure S10). Figure S11 shows the potential energy surfaces for formic acid electro-oxidation on both model surfaces through the carboxyl (COOH)-mediated and formate (HCOO)-mediated paths. It can be found that HCOO is isoenergetic with COOH on Pd(211), while COOH is more stable than HCOO by 0.34 eV on Pd(100). These results imply that Pd RBPs should be more active than Pd cubes because HCOO is preferentially stabilized on the Pd(211) facets, which drives the reaction through the HCOO-mediated pathway and decreases the formation of site-blocking CO (see the caption of Figure S11 for detailed explanations).

In summary, we have demonstrated a facile approach, based on polyol reduction, to the synthesis of single-twinned Pd RBPs by introducing I^- ions into the reaction system as an oxidative etchant for selective removal of multiple-twinned Pd particles and as a capping agent for binding to the Pd{100} facets. The key was to optimize the strength of an oxidative etchant to by adjusting the concentration of I^- ions. The as-prepared Pd RBPs could serve as seeds to produce more complicated single-twinned Pd nanocrystals. When compared with single-crystal Pd nanocubes of similar sizes and commercial Pd black, the Pd RBPs exhibited substantially enhanced catalytic activities toward the formic acid oxidation reaction. Considering their unique shape and structure, as well as the superior catalytic activity, we believe that the Pd RBPs presented here may be promising candidates for shape-controlled synthesis of metal nanocrystals under the influence of a twin defect and for catalysis of various types of reactions.

■ ASSOCIATED CONTENT

Supporting Information

Experimental details, computational studies, TEM images, schematic drawing of right bipyramid, XPS spectra, Cu_{UPD} curves, and catalytic stabilities of Pd nanocrystals. This material is available free of charge via the Internet at http://pubs.acs.org.

■ AUTHOR INFORMATION

Corresponding Author

younan.xia@bme.gatech.edu

Notes

The authors declare no competing financial interest.

■ ACKNOWLEDGMENTS

This work was supported in part by the NSF (DMR-1215034), a DOE grant awarded to the University of Wisconsin-Madison (DE-FG02-05ER15731), and startup funds from Georgia Institute of Technology.

■ REFERENCES

(1) (a) Nishihata, Y.; Mizuki, J.; Akao, T.; Tanaka, H.; Uenishi, M.; Kimura, M.; Okamoto, T.; Hamada, N. *Nature* **2002**, *418*, 164. (b) Zhang, H.; Jin, M.; Xiong, Y.; Lim, B.; Xia, Y. *Acc. Chem. Res.* **2013**, *46*, 1783. (c) Antolini, E. *Energy Environ. Sci.* **2009**, *2*, 915. (d) Yin, L. X.; Liebscher, J. *Chem. Rev.* **2007**, *107*, 133. (e) Kim, S.-W.; Kim, M.; Lee, W. Y.; Hyeon, T. *J. Am. Chem. Soc.* **2002**, *124*, 7642. (f) Adams, B.; Chen, A. *Mater. Today* **2011**, *14*, 282.

(2) (a) Narayanan, R.; El-Sayed, M. A. *Nano Lett.* **2004**, *4*, 1343. (b) Xie, S.; Choi, S.-I.; Xia, X.; Xia, Y. *Curr. Opin. Chem. Eng.* **2013**, *2*, 142. (c) Cheong, S.; Watt, J. D.; Tilley, R. D. *Nanoscale* **2010**, *2*, 2045.

(3) (a) Xiong, Y.; Cai, H.; Wiley, B. J.; Wang, J.; Kim, M. J.; Xia, Y. *J. Am. Chem. Soc.* **2007**, *129*, 3665. (b) Lim, B.; Xiong, Y.; Xia, Y. *Angew. Chem., Int. Ed.* **2007**, *46*, 9279. (c) Xiong, Y.; Cai, H.; Yin, Y.; Xia, Y. *Chem. Phys. Lett.* **2007**, *440*, 273. (d) Huang, X.; Zheng, N. *J. Am. Chem. Soc.* **2009**, *131*, 4602. (e) Xiong, Y.; Washio, I.; Chen, J.; Cai, H.; Li, Z.-Y.; Xia, Y. *Langmuir* **2006**, *22*, 8563. (f) Huang, X.; Tang, S.; Mu, X.; Dai, Y.; Chen, G.; Zhou, Z.; Ruan, F.; Yang, Z.; Zheng, N. *Nat. Nanotechnol.* **2011**, *6*, 28.

(4) (a) Wiley, B. J.; Xiong, Y.; Li, Z.-Y.; Yin, Y.; Xia, Y. *Nano Lett.* **2006**, *6*, 765. (b) Zhang, J.; Li, S.; Wu, J.; Schatz, G. C.; Mirkin, C. A. *Angew. Chem., Int. Ed.* **2009**, *48*, 7787. (c) Wu, H.-L.; Kuo, C.-H.; Huang, M. H. *Langmuir* **2010**, *26*, 12307.

(5) (a) Xiong, Y.; Chen, J.; Wiley, B.; Xia, Y.; Aloni, S.; Yin, Y. *J. Am. Chem. Soc.* **2005**, *127*, 7332. (b) Xiong, Y.; McLellan, J.; Yin, Y.; Xia, Y. *Angew. Chem., Int. Ed.* **2007**, *46*, 790. (c) Lim, B.; Jiang, M.; Tao, J.; Camargo, P.; Zhu, Y.; Xia, Y. *Adv. Funct. Mater.* **2009**, *19*, 189.

(6) Peng, H.-S.; Xie, S.; Park, J.; Xia, X.; Xia, Y. *J. Am. Chem. Soc.* **2013**, *135*, 3780.

(7) (a) Jana, N. R.; Gearheart, L.; Murphy, C. J. *J. Phys. Chem. B* **2001**, *105*, 4065. (b) Sun, Y.; Gates, B.; Mayers, B.; Xia, Y. *Nano Lett.* **2002**, *2*, 165−168.

(8) (a) Xia, Y.; Xiong, Y.; Lim, B.; Skrabalak, S. E. *Angew. Chem., Int. Ed.* **2009**, *48*, 60. (b) Wiley, B.; Sun, Y.; Mayers, B.; Xia, Y. *Chem.—Eur. J.* **2005**, *11*, 454.

(9) (a) Xia, X.; Zeng, J.; Oetjen, L. K.; Li, Q.; Xia, Y. *J. Am. Chem. Soc.* **2011**, *134*, 1793. (b) Langille, M. R.; Zhang, J.; Mirkin, C. A. *Angew. Chem., Int. Ed.* **2011**, *50*, 3543. (c) Pietrobon, B.; McEachran, M.; Kitaev, V. *ACS Nano* **2009**, *3*, 21. (d) Lv, T.; Wang, Y.; Choi, S.-I.; Chi, M.; Tao, J.; Pan, L.; Huang, C.; Zhu, Y.; Xia, Y. *ChemSusChem* **2013**, DOI: 10.1002/cssc.201300479. (e) Zeng, J.; Xia, X.; Rycenga, M.; Henneghan, P.; Li, Q.; Xia, Y. *Angew. Chem., Int. Ed.* **2011**, *50*, 224.

(10) Xia, X.; Xie, S.; Liu, M.; Peng, H.-C.; Lu, N.; Wang, J.; Kim, M. J.; Xia, Y. *Proc. Natl. Acad. Sci. U.S.A.* **2013**, *110*, 6669.

(11) (a) Chierchie, T.; Mayer, C. *Electrochim. Acta* **1988**, *33*, 341. (b) Okada, J.; Inukai, J.; Itaya, K. *Phys. Chem. Chem. Phys.* **2001**, *3*, 3297.

(12) Cuesta, A.; Kibler, L. A.; Kolb, D. M. *J. Electroanal. Chem.* **1999**, *466*, 165.

(13) Shao, M.; Odell, J.; Humbert, M.; Yu, T.; Xia, Y. *J. Phys. Chem. C* **2013**, *117*, 4172.